

Shape coexistence and high spin states in ^{52}Cr

Rajesh Kumar, S. K. Chamoli, and I. M. Govil

Department of Physics, Panjab University, Chandigarh 160014, India

A. Dhal, R. K. Sinha, and L. Chaturvedi

Department of Physics, Banaras Hindu University, Banaras, India

Z. Naik

Tata Institute of Fundamental Research, Mumbai 400005, India

C. R. Praharaj

Institute of Physics, Bhubaneswar 751005, India

S. Muralithar, R. P. Singh, N. Madhavan, P. Sugathan, J. J. Das, and R. K. Bhowmik

Inter University Accelerator Centre, P. O. Box 10502, New Delhi 110067, India

(Received 14 February 2007; published 4 September 2007)

High spin states in ^{52}Cr have been populated by means of the reaction $^{27}\text{Al}(^{28}\text{Si}, 3p)^{52}\text{Cr}$ at a beam energy of 70 MeV and studied with an array, consisting of eight Compton-suppressed clover germanium detectors. Eleven new γ rays have been assigned to ^{52}Cr and placed in the level scheme. The level structure of ^{52}Cr has been extended up to $E_x \approx 10$ MeV. Spins and parities have been assigned to many of the levels on the basis of directional correlations and linear polarization measurements. The band structures are discussed in the framework of cranked Woods-Saxon and deformed Hartree-Fock (HF) models. Both the oblate and prolate orbits are considered for J projection in the HF model. The $K = 0^+$ band is properly understood if we consider the J projection from both prolate and oblate orbits and collectivity shown by the $K = 4^+$ band to be accounted for by taking the J projection from prolate HF configurations. Thus there is prolate and oblate shape coexistence in ^{52}Cr .

DOI: [10.1103/PhysRevC.76.034301](https://doi.org/10.1103/PhysRevC.76.034301)

PACS number(s): 23.20.Lv, 23.20.En, 25.70.Hi, 27.40.+z

I. INTRODUCTION

Most of the nuclei from ^{40}Ca to ^{56}Ni are well described by a shell model in which the most important configurations are $(f_{7/2})^n$ and $(f_{7/2})^{n-r}(f_{5/2}p_{3/2}p_{1/2})^r$, where $(r = 1, 2, \dots)$ [1–3]. Yrast spectroscopy of the majority of fp -shell nuclei follows the shell model expectation, exhibiting somewhat irregular level spacings, often with a marked discontinuity at the termination of the $f_{7/2}$ band of states at $J_{\max} = \frac{1}{2}[(Z - 20)(28 - Z) + (N - 20)(28 - N)]$. This is particularly apparent in the nuclei near N or $Z = 20, 28$, where J_{\max} is not large. At the middle of shell, near ^{48}Cr for which $J_{\max} = 16$, a different structure appears. Low spin levels roughly follow a $J(J + 1)$ energy rule and large $B(E2)$ values occur; the two features together suggest collective rotation. At higher spin, but well below J_{\max} , irregularities in the level spacing occur. These may be taken as evidence of either a level crossing with consequent backbending or, alternatively, a breakdown of collectivity and reappearance of the single-particle structure. Therefore the study of high spin states in $N \approx Z$ $f_{7/2}$ nuclei is an interesting one.

Studies of fp -shell nuclei at or near the neutron shell closure with $N = 28$ is of special interest since these nuclei are ideal for the description in the framework of the shell model. The excited states of these fp -shell nuclei, including those with fairly large spins, have been interpreted in terms of pure shell model configurations [4–7]. Recent important

improvements, both theoretical and experimental, have allowed us to understand different properties such as collective behavior, band termination, backbending, spherical-deformed shape coexistence, and other related phenomena. Coexistence between spherical and deformed shapes can take place rather predominantly in and near semimagic or doubly magic nuclei. In general, a closed magic shell leads to a spherical configuration for the yrast states, whereas the coexisting deformed mode is produced by breaking the magic shell. Recently, such a spherical-deformed shape coexistence has been experimentally found in the doubly magic nucleus ^{56}Ni [8] and was also suggested for ^{52}Cr and ^{54}Fe by Mizusaki *et al.* [9]. The nucleus ^{52}Cr has been studied earlier [10–13] but the band structure has not been properly identified. The purpose of the present investigations is to extend the available information on excited states in ^{52}Cr through heavy-ion-induced reactions and to resolve the ambiguities regarding the spin and parity assignment for the high spin states in this nucleus.

II. EXPERIMENTAL DETAILS AND DATA ANALYSIS

High spin states in the ^{52}Cr nucleus were populated using the $^{27}\text{Al}(^{28}\text{Si}, 3p)^{52}\text{Cr}$ fusion evaporation reaction at a beam energy of 70 MeV. The beam was provided by the 15UD Pelletron facility at the Inter University Accelerator Centre (IUAC, formerly the Nuclear Science Centre), New Delhi,

India. An isotopically enriched $500 \mu\text{g}/\text{cm}^2$ thick ^{27}Al target was used. The de-exciting γ rays were detected by using the Indian National Gamma Array (INGA) at IUAC. For this experiment, the INGA comprised eight Compton-suppressed clover detectors. The efficiency for a clover detector (after add-back) used in the array is typically around 0.17% (photopeak) at ≈ 1 MeV [14,15]. A set of four detectors was placed at 80° ($\phi = \pm 18^\circ$) and another set at 140° ($\phi = \pm 18^\circ$) with respect to the beam direction. A total of about 400 million two- or higher fold γ - γ coincidence events were collected in the experiment. Efficiency and energy calibration were performed with the standard γ -ray ^{152}Eu and ^{133}Ba radioactive sources. After gain-matching, the coincidence events were sorted into symmetric and asymmetric (angle-dependent) matrices for detailed off-line analysis. The data were analyzed by using both RADWARE [16] and IUCSORT [17] computer programs.

Information about γ -ray multiplicities was deduced from directional correlation (DCO) ratios [18,19]. For this purpose, γ - γ matrices were constructed where one axis corresponded to a γ ray recorded by the detectors at 140° and the other axis corresponded to the γ ray recorded by the detectors at 80° . A gate corresponding to a γ ray of known multipolarity was taken on one axis (say, the x axis) and the coincident spectrum was projected on the other axis. Next the same gate was set on the y axis and the projection was made along the x axis. Using gates of known quadrupole transitions, we define R_{DCO} as

$$R_{\text{DCO}} = \frac{I_{\gamma_1 \text{ at } 140^\circ, \text{ gated with } \gamma_2 \text{ at } 80^\circ}}{I_{\gamma_1 \text{ at } 80^\circ, \text{ gated with } \gamma_2 \text{ at } 140^\circ}}. \quad (1)$$

The measured values of R_{DCO} are included in Table I. By assuming stretched transitions, the intensities of the transitions that had the same multipolarity as the gated γ ray was approximately the same in both spectra. For γ rays of different multipolarity, the intensities differed by a factor of almost 2. The R_{DCO} value for the known dipole transitions is ≈ 0.72 and is ≈ 1.2 for quadrupoles by using gates on known quadrupole transitions. These values were cross-checked for self-consistency.

The multipolarity assignments were further corroborated by extracting the electromagnetic character of the transitions by measuring the linear polarization of the γ rays. The linear polarization of the γ rays can be detected through Compton scattering. The differential scattering cross section of the Compton process is given by the Klein-Nishina formula [20]

$$\frac{d\sigma}{d\Omega} = \frac{r_0^2}{2} \left(\frac{E}{E'} \right)^2 \left[\frac{E}{E'} + \frac{E'}{E} - 2 \sin^2 \theta \cos^2 \phi \right], \quad (2)$$

where E and E' are the energies of the incoming and outgoing photon, respectively, r_0 is the classical electron radius, θ is the angle of the outgoing photon with respect to the incident photon, and ϕ is the angle made by electric vector of the incident γ ray with respect to the scattering plane. The use of clover detectors facilitated polarization measurements [21–24]. The individual crystals are considered as a scatterer and the two adjacent crystals as the observers, within a single clover detector. For coincidence polarization measurements the directional correlation from oriented nuclei (IPDCO) procedure [20–22] was applied. The list mode data

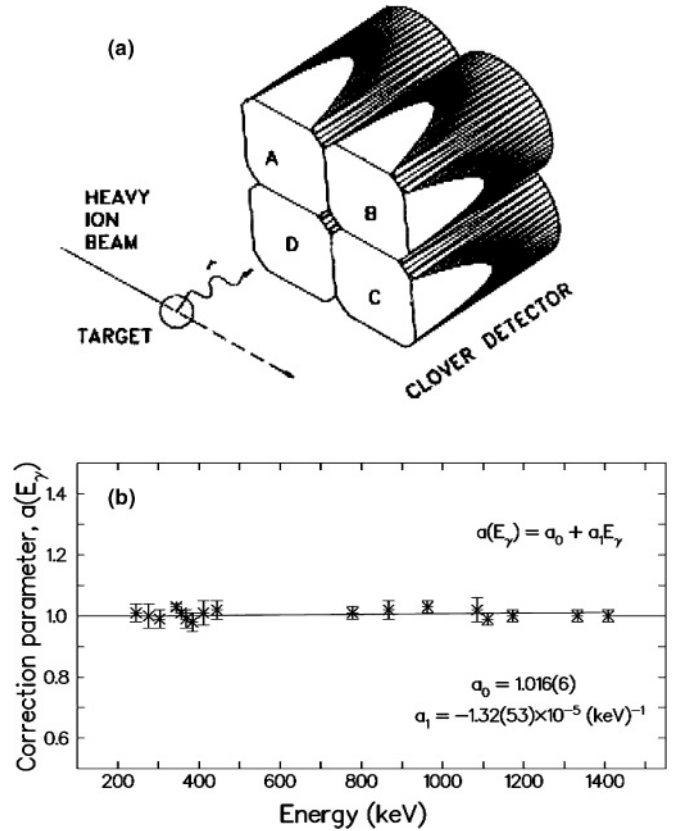


FIG. 1. (a) Schematic diagram of a clover detector consisting of four coaxial HPGc crystals. The letters A, B, C, and D are used to label the different segments of the clover as used in the text. (b) The plot of correction factor a in the IPDCO measurement as a function of energy (E_γ) for the clover detector array.

are analyzed to identify events in which a γ ray incident on one of the four crystals A undergoes Compton scattering parallel or perpendicular to the reaction plane. Thus, a scattering event from $A \rightleftharpoons B$ and $C \rightleftharpoons D$ [Fig. 1(a)] constitutes N_{\parallel} and can be identified if the sum of the energies in A and B or C and D are equal to incident γ -ray energy. Similarly, the events $B \rightleftharpoons C$ and $A \rightleftharpoons D$ are denoted by N_{\perp} . The twofold coincidence spectra AB , BC , CD , and DA were generated by adding the energies of twofold events. The linear polarization of the radiation can typically be determined through a difference between the number of Compton-scattered γ rays in the reaction plane, N_{\parallel} , and perpendicular to it, N_{\perp} . Two asymmetric polarization matrices were formed by placing events along one axis that contained the energy recorded in any one of the detector, while the other axis corresponded to the energy scattered in a perpendicular or parallel segments of the clover with respect to the beam axis. From the projected spectra, the number of γ rays with scattering axis perpendicular (N_{\perp}) and parallel (N_{\parallel}) to the emission plane were obtained for a given γ ray. From these spectra, the asymmetry parameter Δ_{IPDCO} was obtained from the relation

$$\Delta_{\text{IPDCO}} = \frac{[a(E_\gamma)N_{\perp}] - N_{\parallel}}{[a(E_\gamma)N_{\perp}] + N_{\parallel}}, \quad (3)$$

TABLE I. Excitation energies in keV, initial and final spins for the transitions, γ -ray energies in keV, relative intensities, DCO ratio, and the multipolarity of the transitions belonging to the ^{52}Cr nucleus.

E_i	$J_i^\pi \rightarrow J_f^\pi$	E_γ	I_γ^a	R_{DCO}	Mult.
3113.9	$6^+ \rightarrow 4^+$	346.2			(E2)
2767.9	$4^+ \rightarrow 4^+$	397.7			E2
4015.6	$5^+ \rightarrow 5^+$	400.4	4.0	1.3 (0.041) ^b	$M1+E2^c$
5824.7	$8^+ \rightarrow 7^+$	427.4	13.0	0.8 (0.022) ^b	M1
4038.6	$(4^+) \rightarrow 3^+$	567.3	1.0		(M1)
5396.7	$7^+ \rightarrow 6^+$	591.2	18.6	0.72 (0.026) ^b	M1
4015.6	$5^+ \rightarrow 4^+$	600.4	7.8	0.73 (0.08) ^b	M1
6453.4	$9^+ \rightarrow 8^+$	628.9	9.2	0.65 (0.018) ^b	M1
3415.4	$4^+ \rightarrow 4^+$	647.4	11.6	1.2 (0.072) ^b	$M1+E2^c$
3471.8	$3^+ \rightarrow 4^+$	704.2	2.4	0.66 (0.031) ^b	M1
10159	$(13^+) \rightarrow (12^+)$	720.7			(M1)
3113.9	$6^+ \rightarrow 4^+$	744.4	76.9	1.1 (0.027) ^b	E2
7237.9	$10^+ \rightarrow 9^+$	784.3	30.4	0.57 (0.029) ^b	M1
4805.7	$6^+ \rightarrow 5^+$	790.4	11.0	0.75 (0.016) ^b	M1
3615.9	$5^+ \rightarrow 4^+$	847.9	3.1	0.7 (0.09) ^b	M1
2369.7	$4^+ \rightarrow 2^+$	935.7	100	1.06 (0.08) ^b	E2
8216.5	$11^+ \rightarrow 10^+$	978.5	14.3	0.7 (0.069) ^b	M1
7401.0	$(12^+) \rightarrow (10^+)$	1036.3			(E2)
6453.4	$9^+ \rightarrow 7^+$	1056.4	2.5		(E2)
4805.7	$6^+ \rightarrow 5^+$	1189.8	1.6		($M1+E2$)
9440.4	$(12^+) \rightarrow 11^+$	1222.4	2.6		(M1)
3615.9	$5^+ \rightarrow 4^+$	1245.4			
4015.6	$5^+ \rightarrow 4^+$	1247.7	12.2	0.72 (0.059) ^b	M1
2767.9	$4^+ \rightarrow 2^+$	1333.6	40	1.07 (0.037) ^b	E2
5396.7	$7^+ \rightarrow 5^+$	1381.6	2.9	1.25 (0.094) ^b	E2
1434.2	$2^+ \rightarrow 0^+$	1434.2	140	1.1 (0.02) ^d	E2
6365.4	$10^+ \rightarrow 8^+$	1615.0	1.3		E2
4750.4	$8^+ \rightarrow 6^+$	1636.4	67	1.2 (0.032) ^b	E2
4805.7	$6^+ \rightarrow 6^+$	1692.3			($M1+E2$)
6453.4	$9^+ \rightarrow 8^+$	1702.4	31.8	0.78 (0.039) ^b	M1
8216.5	$11^+ \rightarrow 9^+$	1763.3	2.2	1.1 (0.03)	E2
10159	$(13^+) \rightarrow 11^+$	1943.3	7.7	1.26 (0.083) ^b	E2
3471.8	$3^+ \rightarrow 2^+$	2037.8	3.4		($M1+E2$)
9440.0	$(12^+) \rightarrow 10^+$	2200.4			(E2)
6381.0	$(6^+) \rightarrow 5^+$	2765.0			

^aErrors on the relative intensities are estimated to be less than 5% of the quoted values for strong transitions ($I_\gamma \geq 10$) and less than 20% for the weaker transitions ($I_\gamma < 10$). The values are normalized to 100% for the 936-keV transition of the yrast band.

^b R_{DCO} ratio from the gate on the 1434-keV quadrupole transition.

^cNonstretched $\Delta = 1$ dipole transition.

^d R_{DCO} ratio from the gate on the 936-keV quadrupole transition.

where N_\perp and N_\parallel were the intensities of the scattered photon perpendicular and parallel to the direction of the reaction plane, respectively. The parameter a denotes the correction from the asymmetry in the response of the clover segments. This correction, defined as

$$a(E_\gamma) = \frac{N_\parallel(\text{unpolarized})}{N_\perp(\text{unpolarized})}, \quad (4)$$

was determined as a function of γ -ray energy by using a ^{152}Eu source. Figure 1(b) shows the variation of a with energy E_γ . It

was fitted with the expression $a(E_\gamma) = a_0 + a_1 E_\gamma$, resulting in $a_0 = 1.016(6)$ and $a_1 = -1.32(53) \times 10^{-5}$, where E_γ is in keV. As is clear from Fig. 1(b), the value of a is almost constant and close to unity, showing very little asymmetry in horizontal and vertical segments. This involves all the clover detectors placed in the reaction plane so that we may get a measurable polarization for the weak transitions. An electric transition results in a positive value for Δ_{IPDCO} whereas a negative value corresponds to a magnetic transition. A near-zero value is indicative of a possible admixture. As we use

the data from detectors at all angles in the reaction plane, we cannot perform quantitative polarization measurements. However, we may get useful information about the nature of the γ ray of interest [22,24]. The polarization sensitivity is measured by measuring the asymmetry parameter (Δ_{IPDCO}) and verifying the multipolarity for the well-known $E2$ and $M1$ transitions.

III. RESULTS AND DISCUSSION

The level scheme of ^{52}Cr resulting from the present work is shown in Fig. 2. The transitions and their placement in the level scheme have been determined by γ -ray intensities, γ - γ coincidences, reverse gating, and sum energy relations. The width of the arrows are approximately equal to the intensities as obtained from the coincident spectra of the lowest transition,

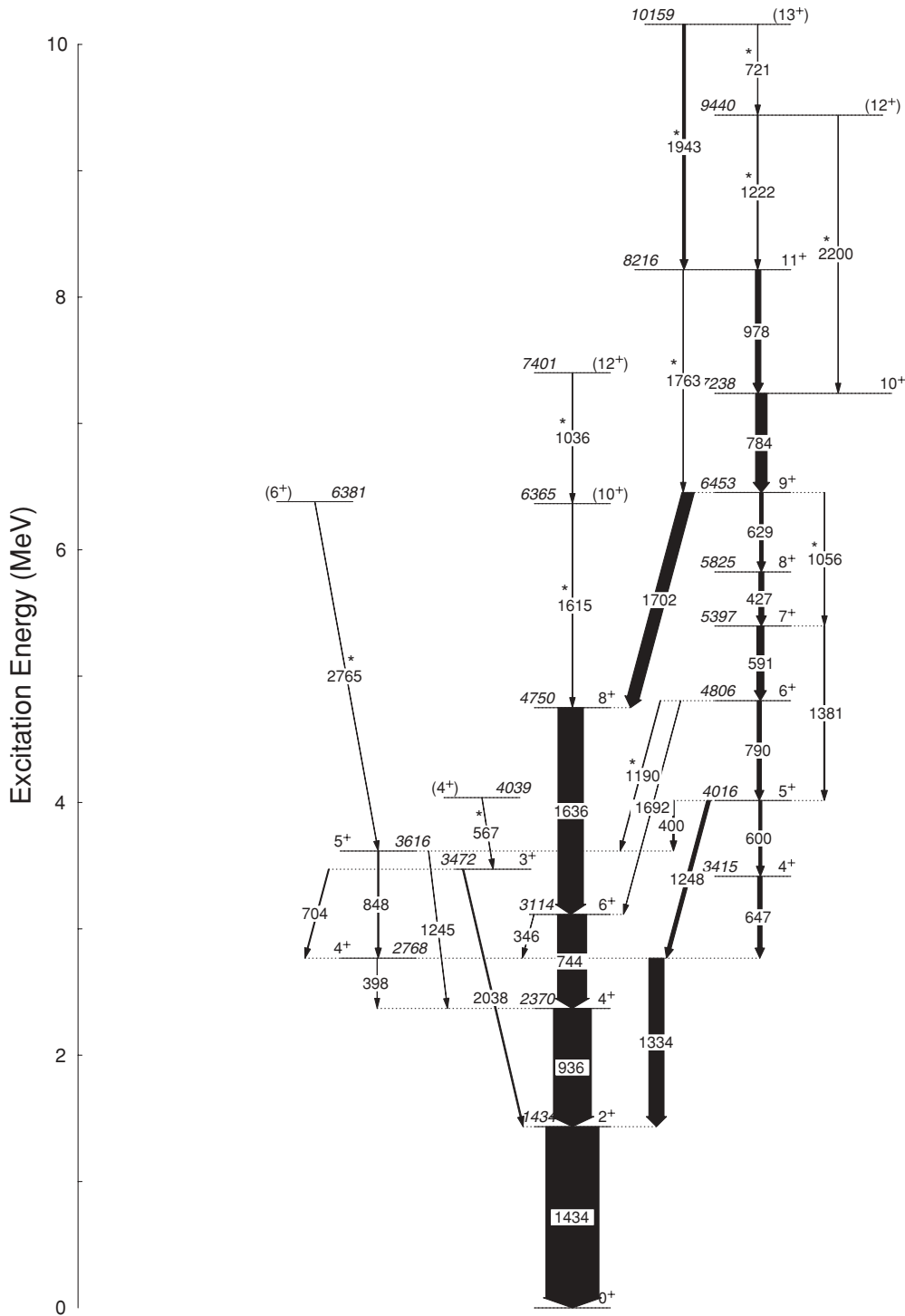


FIG. 2. Level scheme for ^{52}Cr populated in the $^{27}\text{Al}(^{14}\text{Si}, p3n)^{52}\text{Cr}$ reaction. Newly observed transitions are marked with an asterisk. The energies are marked within ± 1 keV. The spin and parity assignments, given in parentheses, are tentative.

1434 keV ($2^+ \rightarrow 0^+$). The γ -ray energies, relative intensities, spin, parity, and multipolarity of the γ transitions based on R_{DCO} ratios and polarization measurements are given in Table I. In the present experiment, the level structure of ^{52}Cr has been established up to $E_x \approx 10$ MeV and up to spin $J \approx 13\hbar$. In addition to the transitions reported by Banerjee *et al.* [13], eleven new transitions have been identified in the present work. These transitions are marked by asterisks in the level scheme. The 346-keV γ -ray transition has not been observed by Banerjee *et al.* [13] but was reported earlier by Sprague *et al.* [10]. We have also observed this γ -ray transition in our present measurement. The representative spectra, gated on transitions 1434, 427, and 784 keV corresponding to different bands, are shown in Fig. 3. The spectrum in Fig. 3(a) is obtained by gating on 1434-keV transitions in the γ - γ matrix. The established irregular ground-band transitions up to 8^+ have been confirmed, though the primary discrete feeding to this band is via an apparent dipole transition at $E_\gamma = 1702$ keV. Two more weak transitions of 1615 and 1036 keV

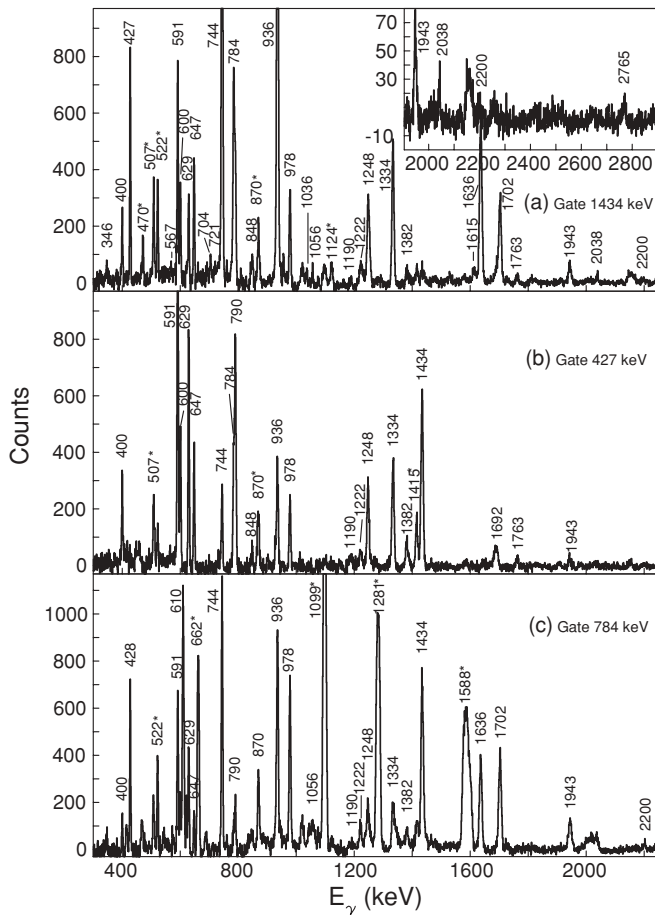


FIG. 3. γ - γ coincidence spectra: (a) spectrum obtained by setting gate on 1434 keV, (b) spectrum obtained by setting gate on 427 keV, and (c) spectrum obtained by setting gate on 784 keV, respectively. The transitions marked with asterisks belong to the neighboring nuclei. (The transitions 610, 662, 1099, and 1281 keV belong to the ^{50}Cr nucleus, the transitions of energy 870 and 1415 keV belong to the ^{52}Mn nucleus, and 507 and 522 keV belong to the background.)

have been identified in ground-state band extending its spin up to (12^+). The transitions at 567, 721, 1190, 1056, and 2765 keV are the newly observed transitions. The placement of the 2038- and 704-keV γ transitions depopulating the 3472-keV level is consistent with earlier results [11,13]. Another irregular band built on the 2768-keV level has been extended to a tentative spin of (13^+) and the new transitions (1056, 1222, 1763, 1943, and 2200 keV) placed in this band can be seen in Figs. 3(b) and 3(c), which were obtained by gating on 427- and 784-keV transitions, respectively. In contrast to the results of Brinde *et al.* [11], the present results do not support the possibility of existence of two closely lying levels at 6452.4 and 6453.4 keV. In spite of two close lying levels, one level at energy 6453 keV has been observed that decays simultaneously by 1702- and 629-keV transitions. This result is based on the fact that the 784-keV transition is observed in coincidence with the 629-, 427-, 1702-, 744-, 935-, and 1434-keV transitions. This can be clearly seen from the spectrum in Fig. 3(c). We have also observed that the transition of 629 keV is not a doublet, which was suggested by Brinde *et al.* [11].

We have performed R_{DCO} and polarization measurements for almost all the observed γ transitions. The results of polarization measurements are shown in Fig. 4. On the basis of the DCO and linear polarization analysis, stretched $E2$ and quadrupole character are assigned to the 1434-, 936-, 1334-, 744-, 1636-keV γ rays. The transitions of 1615 and 1036 keV are too weak to obtain information on their multiplicities. As these γ rays continue the rotational sequence, they are assumed to be stretched $E2$ transitions and tentative $I^\pi = (10^+)$ and (12^+) spin-parity values are assigned to the states at 6365 and 7401 keV, respectively. The γ transition of 848 keV is assigned an $M1$ nature from the present DCO and polarization measurements. The transition of 704 keV is assigned dipole character from the measured DCO ratio. We have assigned $I^\pi = 4^+$ to the 3415-keV level (decaying by a 647-keV γ ray), in agreement with previous work [11–13]. On the basis of DCO value and polarization measurement, we adopt a nonstretched $\Delta I = 0$, $M1 + E2$ multipolarity for the 647-keV transition. The level with 4016 keV energy has previously been assigned $I^\pi = 5^+$ [13]. Our DCO values are consistent with this spin assignment. The γ transition of 600 keV depopulating this level has been assigned $M1$ on the basis of DCO and IPDCO measurements. No linear polarization could be measured for the 400- and 1248-keV decay γ rays from the 4016-keV level because of the overlapping γ ray. However, the DCO ratio indicates a nonstretched $\Delta I = 0$, $M1 + E2$ multipolarity for 400 keV and dipole character for the 1248-keV γ -ray transition. Our assignment of $I^\pi = 6^+$ for the 4806-keV level confirms the value suggested by Banerjee *et al.* [13] on the basis of the $M1$ nature of the 790-keV transition. The analysis of the data obtained for the transitions of 790, 591, 427, 629, 784, 978, and 1702 keV shows also that these γ rays are essentially magnetic dipoles. The 1943-keV transition γ ray is assigned a stretched $E2$ on the basis of the DCO and polarization measurements. For some of the transitions between the highest lying levels, the angular correlations and linear polarization could not be measured accurately because of the lack of statistics.

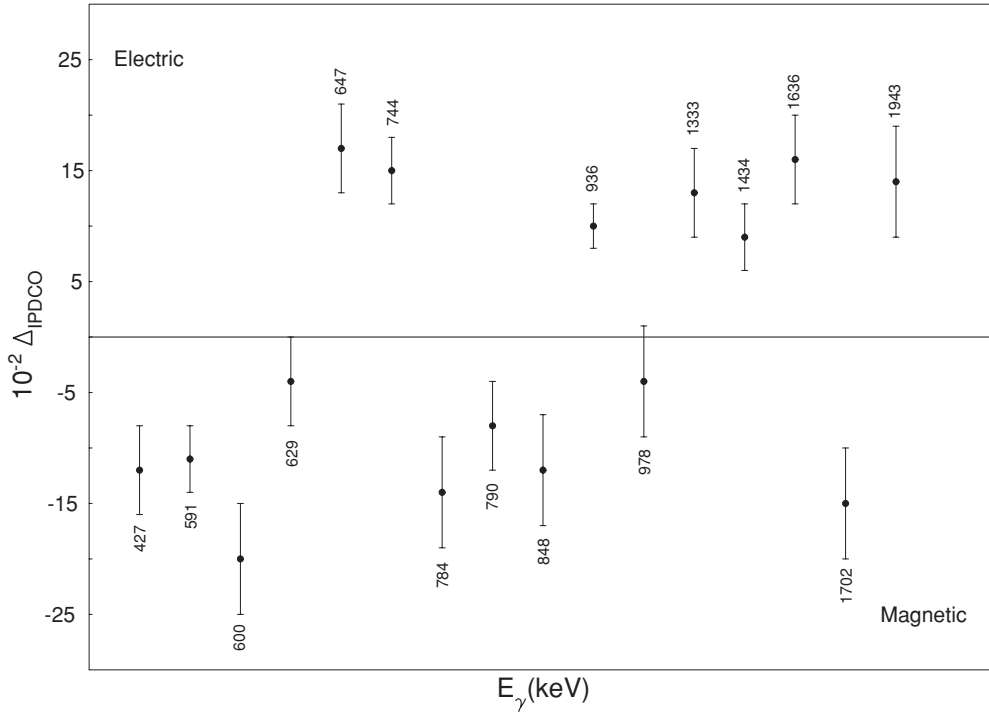


FIG. 4. Experimental γ -ray asymmetry parameter Δ_{IPDCO} , from polarization measurements plotted for γ -ray transitions of ^{52}Cr . A positive value corresponds to an electric transition and a negative value indicates the magnetic transition. The quoted errors are due to peak fitting and background subtraction.

A. Comparison with Hartree-Fock microscopic model

The band structure of the ^{52}Cr nucleus has been studied with the deformed Hartree-Fock (HF) model and angular momentum (J) projection [25,26]. This is a useful microscopic model to study the spectra and the electromagnetic transition probabilities in well-deformed as well as moderately deformed nuclei [25–31]. The deformed HF equation is derived from the nuclear Hamiltonian, which consists of single-particle and residual two-body interaction terms:

$$H = \epsilon + V, \quad (5)$$

where, schematically, ϵ stands for single-particle energies of spherical shell model orbits and V stands for pp , pn , and nn two-body residual interactions. The surface delta interaction is considered as a residual interaction among the active nucleons with interaction strength $V_{pp} = V_{np} = V_{nn} = 0.5$ MeV. We have taken $p_{1/2}$, $p_{3/2}$, $f_{5/2}$, $f_{7/2}$, and $g_{9/2}$ orbits above a $Z = N = 20$ spherical closed shell with spherical single-particle energies of 1.8, 0., 0.57, 4.6, and 5.8 MeV, respectively (with the same single-particle energies taken for protons and neutrons) for HF and J projection calculations. Axial symmetry of the HF field is assumed in this theoretical analysis.

Deformed HF orbits are obtained from the self-consistent solution of the HF equation [25,27]. The intrinsic states $|\phi_K\rangle$ are constructed by making appropriate particle-hole arrangement on the proton and neutron HF orbits near the Fermi surfaces. Because of axial symmetry of the HF field, an intrinsic state is a state of good K but not of good J . To study the spectra and electromagnetic matrix elements of the bands,

we need good J states. The good angular momentum states of a given $|\phi_K\rangle$ are obtained by J projection. The J projection operator is [25]

$$P_K^{JM} = \frac{2J+1}{8\pi^2} \int d\Omega D_{MK}^J(\Omega) R(\Omega), \quad (6)$$

where $R(\Omega)$ is the rotation operator and Ω stands for the Euler angles.

The matrix element of the Hamiltonian between the projected states of J obtained from intrinsic states ϕ_{K_1} and ϕ_{K_2} is

$$H_{K_1 K_2}^J = \frac{2J+1}{2} \frac{1}{(N_{K_1 K_1}^J N_{K_2 K_2}^J)^{1/2}} \times \int_0^\pi d\beta \sin \beta d_{K_1 K_2}^J(\beta) \langle \phi_{K_1} | H e^{-i\beta J_y} | \phi_{K_2} \rangle, \quad (7)$$

where

$$N_{K_1 K_2}^J = \frac{2J+1}{2} \int_0^\pi d\beta \sin \beta d_{K_1 K_2}^J(\beta) \langle \phi_{K_1} | e^{-i\beta J_y} | \phi_{K_2} \rangle \quad (8)$$

is the amplitude overlap for angular momentum J .

In general, two states $|\Psi_{K_1}^{JM}\rangle$ and $|\Psi_{K_2}^{JM}\rangle$ projected from two intrinsic configurations $|\phi_{K_1}\rangle$ and $|\phi_{K_2}\rangle$ are not orthogonal to each other, even if the intrinsic states $|\phi_{K_1}\rangle$ and $|\phi_{K_2}\rangle$ are orthogonal. When necessary we orthonormalize for each J and then diagonalize using the equation (see Ref. [27])

$$\sum_{K'} (H_{KK'}^J - E_J N_{KK'}^J) C_{K'}^J = 0, \quad (9)$$

Prolate HF orbits for ^{52}Cr

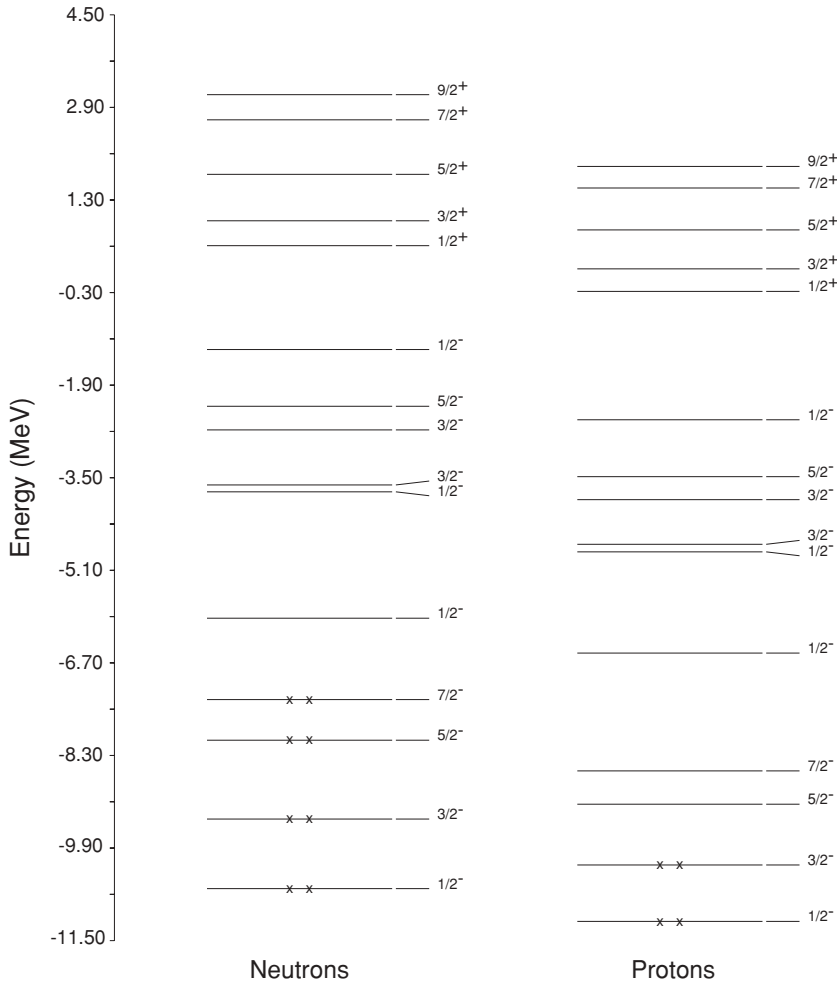


FIG. 5. The prolate deformed Hartree-Fock orbits for protons and neutrons.

where C_K^J are the orthonormalised amplitudes, which can be identified as the band-mixing amplitudes.

For ^{52}Cr , four active protons and eight active neutrons are considered above the $N = Z = 20$ core and the HF calculation is performed. The prolate HF orbits for protons and neutrons are shown in Fig. 5. Both the oblate and the prolate HF solutions are considered for J projection and band-mixing calculations. Since the two-body interaction is used in obtaining the self-consistent HF orbits, mixing of a small number of intrinsic configurations can, after J projection, describe the low-energy spectra and bands [30,32].

The following intrinsic configurations are considered for angular momentum projection and band mixing calculation:

- (i) oblate configurations:
 - (A) $K = 0^+$ (HF) and (B) $K = 2^+ \nu(1/2^- \otimes 3/2^-)$ and
- (ii) prolate configurations:
 - (C) $K = 0^+$ (HF),
 - (D) $K = 1^+ \pi(5/2^- \otimes -3/2^-)$,
 - (E) $K = 4^+ \nu(7/2^- \otimes 1/2^-)$,
 - (F) $K = 3^+ \nu(5/2^- \otimes 1/2^-)$, and
 - (G) $K = 5^+ \nu(7/2^- \otimes 1/2^-) \otimes \pi(5/2^- \otimes -3/2^-)$.

We have considered two different sets of band mixing for the ground band. In the first case we have mixed the configurations A , B , C , and D , that is, prolate-oblate band mixing [denoted as Th(1) in Fig. 6]. In the second case [Th(2)], we consider only the oblate band mixing (configurations A and B). The lowest band after these two band mixings are compared with the experimental ground band in Fig. 6. In the Th(1) case, high spin states up to $J^\pi = 4^+$ are dominated by configuration C (prolate $K = 0^+$ band). The state $J^\pi = 6^+$ is well mixed between prolate and oblate $K = 0^+$ bands. The state $J^\pi = 8^+$ is mainly dominated by configuration A and states $J^\pi = 10^+$ and 12^+ are dominated by configuration B . In the case of Th (2), high spin states up to $J^\pi = 8^+$ are mainly of oblate configuration A and states above this are of configuration B . Both Th(1) and Th(2) give reasonable explanation of the ground-band spectrum. The calculated $B(E2)$ values for Th(1) and Th(2) are 0.0135 and 0.0066 ($e b$)², respectively.

The lowest band after the mixing of configurations E , F , and G is compared with the excited $K = 4^+$ experimental band in Fig. 6. In this band, high spin states up to $J^\pi = 9^+$ are dominated by configuration E and states higher than $J^\pi = 9^+$ are dominated by configuration G . For this $K = 4^+$ band we have

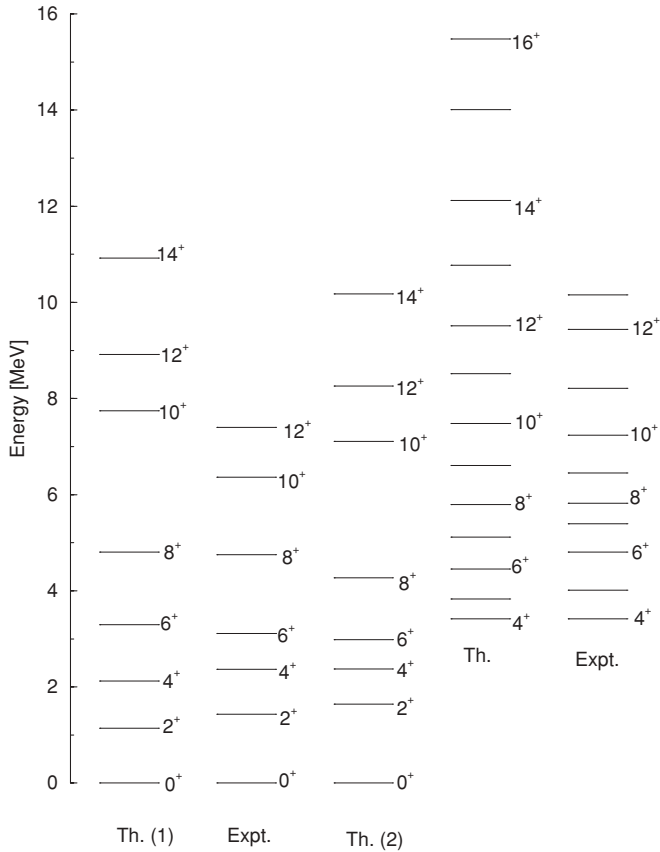


FIG. 6. Comparison of experimental levels with the results of the microscopic deformed Hartree-Fock model.

considered the prolate configurations because the collectivity shown by this band is only understood by J projection from the prolate ones. Among the oblate configurations only $K = 0^+$ (configuration A) shows some regular rotational feature; none of the other possible oblate configurations show the collective excitation (i.e., regular pattern in the spectrum) observed in the experimental $K = 4^+$ band. The quadrupole moment (Q_0) of the $K = 4^+$ bandhead obtained in our calculation for this band is $0.903 e b$ whereas for the ground band it is $0.785 e b$. So the band structures seen in ^{52}Cr involve moderately deformed bands. The excited $K = 4^+$, where one neutron is excited from the $\Omega^\pi = 7/2^-$ to the $1/2^-$ prolate neutron orbit across the neutron Fermi surface, drives the nucleus toward more prolate deformation.

B. Comparison with the cranked Woods-Saxon model

To understand the prolate oblate shape coexistence, total Routhian surface (TRS) calculations have been performed within the Wood-Saxon cranking formalism [33,34] for ^{52}Cr . For these calculations the average mean field is taken to be a rotating Wood-Saxon potential [35,36] with a monopole type of pairing interaction. The pairing Δ and the Fermi level λ are found self-consistently by using the Bardeen-Cooper-Schrieffer (BCS) equation [37]. The pairing gap Δ is allowed to vary smoothly as a linear function of ω in such a way that it becomes $\Delta_0/2$ at the critical frequency ω_c , where

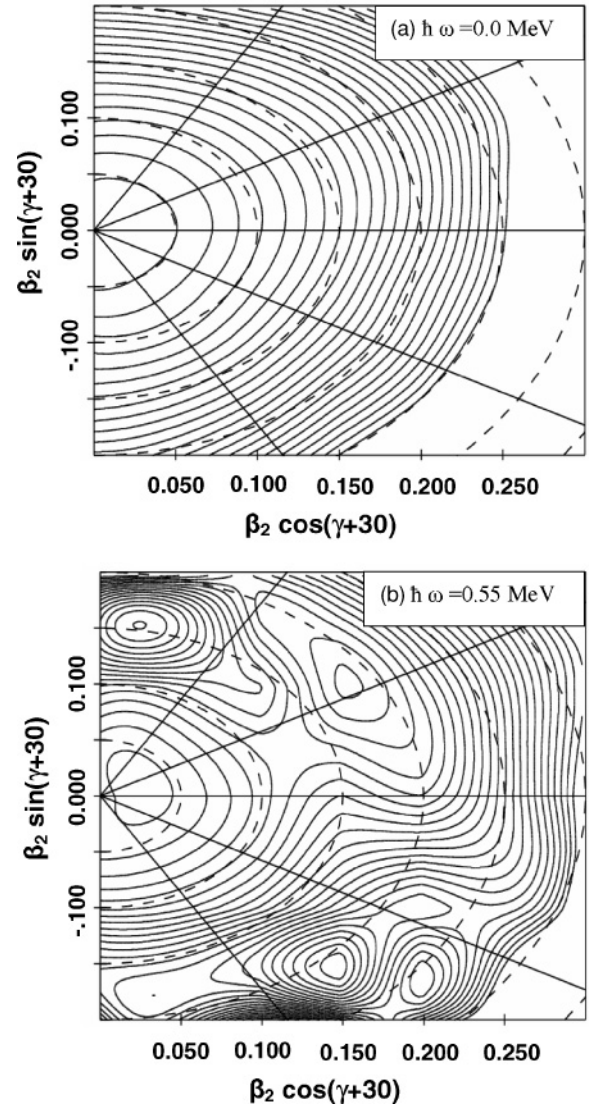


FIG. 7. Total Routhian surface plots in β_2 - γ plane for the positive-parity band in ^{52}Cr for the rotational frequencies $\hbar\omega = 0.0$ MeV (a) and $\hbar\omega = 0.55$ MeV (b). The energy separation between the contours is 250 keV.

Δ_0 is the pair gap at $\omega = 0.0$. Values of $\hbar\omega_c^\pi = 1.15$ MeV for protons and $\hbar\omega_c^\nu = 0.95$ MeV for neutrons are taken for nuclei in this mass region. The Strutinsky-shell-corrected [38] single-particle energies are used to include the microscopic quantal effects. This corrected total energy of the nucleus in the rotating frame is then minimized with respect to three deformation parameters, β_2 , γ , and β_4 . The TRS results are plotted in Fig. 7 for the frequencies $\hbar\omega = 0.0$ and $\hbar\omega = 0.55$ MeV, respectively. We have seen that the TRS plot for the ground state ($\hbar\omega = 0.0$) shows a broad minimum at $\gamma = -30^\circ$ [Fig. 7(a)]. This indicates an oblate structure for the ground-state band with negligible deformation, consistent with the very small value of experimental $B(E2) = 0.0132 (e b)^2$ [39,40]. The ground-state spectrum is consistent with microscopic HF calculation Th(2), also indicating a small oblate deformation. At $\hbar\omega = 0.55$ MeV a sharp prolate minimum for deformation $\beta_2 \sim 0.20$ and $\gamma \sim 0^\circ$ is formed, as shown in

Fig. 7(b), along with a oblate minima with $\beta_2 \sim 0.03$. The other minima shown in Fig. 7(b) are of little consequence because of their very poor intensities. This model therefore also indicates the oblate and prolate shape coexistence at higher excitation, consistent with the projected HF microscopic calculations.

IV. SUMMARY

The level structure of the $N = 28$ even-even ^{52}Cr nucleus has been studied with an eight clover detector array using the $^{28}\text{Si} + ^{27}\text{Al}$ fusion evaporation reaction. Eleven new transitions belonging to this nucleus have been identified, extending the level scheme up to excitation energy of 10 MeV and spins up to $13\hbar$. The observed level scheme is compared with the microscopic projected Hartree-Fock calculation and the results are found to be in reasonably good agreement with theory

considering the mixed configuration for the ground band and the prolate configurations for the excited $K = 4^+$ band. The cranked Woods-Saxon model also suggest a oblate ground-state band with very small deformation, in agreement with a very small experimental $B(E2)$ value.

ACKNOWLEDGMENTS

The authors would like to thank the accelerator crew for providing an excellent beam from the 15UD Pelletron at the Inter University Accelerator Centre, New Delhi. We would also like to thank Dr. G. de Angelis and Professor Umesh Garg for discussion and providing useful suggestions on the present work. Financial support from the UGC-DAE Consortium for Scientific Research, Kolkata, and the CSIR is gratefully acknowledged.

-
- [1] W. Kutschera, B. A. Brown, and K. Ogawa, Riv. Nuovo Cimento **1**, 12 (1978).
- [2] A. Poves and A. Zuker, Phys. Rep. **70**, 235 (1981).
- [3] R. B. Mooy and P. M. W. Glaudemans, Z. Phys. A **312**, 59 (1983).
- [4] K. Lips and M. T. McEllistrem, Phys. Rev. C **1**, 1009 (1970).
- [5] I. P. Johnstone and H. G. Benson, J. Phys. G **3**, L69 (1977).
- [6] A. Yokoyama, T. Oda, and H. Horie, Prog. Theor. Phys. **60**, 427 (1978).
- [7] I. P. Johnstone, Phys. Rev. C **17**, 1428 (1978).
- [8] D. Rudolph *et al.*, Phys. Rev. Lett. **82**, 3763 (1999).
- [9] T. Mizusaki, T. Otsuka, M. Honma, and B. A. Brown, Phys. Rev. C **63**, 044306 (2001).
- [10] S. W. Sprague *et al.*, Phys. Rev. C **4**, 2074 (1971).
- [11] A. Berinde *et al.*, Nucl. Phys. A **284**, 65 (1977).
- [12] D. Evers, A. Harasim, R. L. McGrath, and W. Assmann, Phys. Rev. C **63**, 1690 (1977).
- [13] P. Banerjee, B. Sethi, J. M. Chatterjee, M. B. Chatterjee, and P. Bhattacharya, Phys. Rev. C **36**, 2274 (1987).
- [14] M. Saha Sarkar *et al.*, Nucl. Instrum. Methods Phys. Res. A **491**, 113 (2002).
- [15] Krishichayan *et al.*, Phys. Rev. C **70**, 044315 (2004).
- [16] D. C. Radford, Nucl. Instrum. Methods Phys. Res. A **361**, 297 (1995).
- [17] N. S. Pattabiraman, S. N. Chintalapudi, and S. S. Ghugre, Nucl. Instrum. Methods Phys. Res. A **526**, 432 (2004).
- [18] F. S. Stephens, M. A. Delenplanque, R. M. Diamond, A. O. Macchiavelli, and J. E. Draper, Phys. Rev. Lett. **54**, 2584 (1985).
- [19] C. W. Beausang *et al.*, Nucl. Instrum. Methods Phys. Res. A **364**, 560 (1995).
- [20] H. Morinaga and T. Yamazaki, in *In-Beam Gamma Ray Spectroscopy* (North-Holland, Amsterdam, 1976), p. 105.
- [21] Ch. Droste, Nucl. Instrum. Methods Phys. Res. A **378**, 518 (1996).
- [22] K. Starosta, Nucl. Instrum. Methods Phys. Res. A **423**, 16 (1999).
- [23] G. Duchêne *et al.*, Nucl. Instrum. Methods Phys. Res. A **432**, 90 (1999).
- [24] N. S. Pattabiraman *et al.*, Phys. Rev. C **65**, 044324 (2002).
- [25] G. Ripka, in *Advances in Nuclear Physics* Vol. 1, edited by M. Baranger and E. Vogt (Plenum Press, New York, 1968), Vol. 1, p. 183; D. M. Brink, Proc. Int. School of Physics Course **36**, edited by C. Bloch (Academic Press, 1966), p. 247; M. R. Gunye and C. S. Warke, Phys. Rev. **156**, 1087 (1967).
- [26] Z. Naik and C. R. Prahara, Phys. Rev. C **67**, 054318 (2003).
- [27] C. R. Prahara, J. Phys. G **14**, 843 (1988).
- [28] A. K. Rath, C. R. Prahara, and S. B. Khadkikar, Phys. Rev. C **47**, 1990 (1993); A. K. Rath, P. M. Walker, and C. R. Prahara, J. Phys. G **30**, 1099 (2004).
- [29] S. Chattopadhyay, H. C. Jain, M. L. Jhingan, and C. R. Prahara, Phys. Rev. C **50**, 93 (1994).
- [30] D. P. Ahalpara *et al.*, Nucl. Phys. A **371**, 210 (1981).
- [31] A. Faessler *et al.*, Phys. Rev. **156**, 1064 (1967).
- [32] S. B. Khadkikar, S. C. K. Nair, and S. P. Pandya, Phys. Lett. **B36**, 290 (1971).
- [33] P. Ring and P. Schuck, *The Nuclear Many Body Problems* (Springer-Verlag, Berlin, 1980), p. 244.
- [34] W. Nazarewicz, M. A. Riley, and J. D. Garrett, Nucl. Phys. A **512**, 61 (1990).
- [35] T. R. Werner and J. Dudek, At. Data Nucl. Data Tables **59**, 1 (1995).
- [36] T. R. Werner and J. Dudek, At. Data Nucl. Data Tables **50**, 179 (1992).
- [37] S. G. Nilsson and I. Ragnarsson, *Shapes and Shells in Nuclear Structure* (Cambridge University Press, Cambridge, England, 1995), p. 290.
- [38] V. M. Strutinsky, Yad. Fiz. **3**, 614 (1966); Nucl. Phys. A **95**, 420 (1967).
- [39] R. Ernst *et al.*, Phys. Rev. Lett. **84**, 416 (2000).
- [40] C. W. Towsley *et al.*, Nucl. Phys. A **250**, 381 (1975).